ON THE CHARACTERIZATION AND MECHANISMS OF SHOCK INITIATION IN HETEROGENEOUS EXPLOSIVES

L.G. Hill and R.L. Gustavsen
Los Alamos National Laboratory
Los Alamos, NM 87545

We present a new methodology for fitting *x-t* shock initiation data based upon extended detonation shock dynamics (DSD) theory. Fits are generated by simple, analytic phase plane functions. We demonstrate the technique using recent PBX 9501 and PBX 9502 gas gun data. The method enhances Pop plot and inert Hugoniot accuracy, and provides extended DSD calibration in the initiation regime. It is also useful for studying physical initiation mechanisms. We use it to evaluate the *single curve initiation* model. We then develop an approximately universal fitting function for reaction build-up, from which the c-j reaction zone thickness can be estimated. Finally, we define a practical figure-of-merit to quantify homogeneous/heterogeneous initiation character.

INTRODUCTION

At the time of this writing the shock initiation wedge test has been in use for over 40 years. Data analysis methods have changed little since the first classic studies in 1960.[1,2] Most often one draws a line through the early (approximately inert) *x-t* shock data, and a second line through the late (steadily detonating) data. An inert Hugoniot point is inferred, in part, from the slope of the first line. Detonation transition is taken as the point (t^*, x^*) where the two lines cross. Transition has also been defined as the point on the shock record where the slope first differs perceptibly from that of the steady detonation. Often, methods have been based upon features that can be read directly from the film record.

The problems with traditional methods are that they 1) do not use any definite or repeatable physical criterion, 2) differ in implementation between experimenters, 3) do not use all the record information, 4) have certain systematic errors, and 5) do not take advantage of recent theoretical and computational advances.

Historically, wedge test analysis errors have been eclipsed by experimental ones, the foremost being 1) limited planarity of the plane wave lens, and 2) imperfect and variable pressure support provided by the following flow. Consequently the end result has been somewhat forgiving of analytical approach. Recent refinements in gas gun experimental techniques[3] have substantially reduced the two primary sources of experimental error. Better analysis methods will allow this new class of data to realize its full potential.

The method we explore is motivated by extended detonation shock dynamics (DSD) theory[4]. DSD suggests a class of smooth generating functions of the form $a[U]$, where U is the shock speed and a is its acceleration. Fits generated in this manner can fit *x-t* data in fine detail, thereby expanding its usefulness. First, it helps us to more accurately determine inert Hugoniot and Pop plot curves. Secondly, it allows one to calibrate the extended DSD model in a region far from that covered by current experiments.

Beyond the utilitarian objectives of characterization and calibration, accurate shock trajectory fits can help deduce physical initiation mechanisms. Shock trajectories, together with magnetic particle velocity records, comprise the primary information available for appraising reaction rate models in the initiation regime.

A question that is closely related to reaction rate laws is how well initiation follows the popular *single curve initiation* (SCI) model, upon which the *Forest Fire* reaction rate form[5] is built. SCI is appealing for its utility; however, it has little theoretical motivation to recommend it, and there is disagreement as to how well it works and under what conditions. Accurate shock trajectories can help answer this question.

Another important issue is how various explosives differ as to the nature of their build up to detonation—what has been loosely referred to as the relative degree of "heterogeneity" versus "homogeneity". To date, descriptions have been mostly qualitiative. With sufficiently accurate shock trajectory fits, one is in a position to quantify some of these concepts.

THEORETICAL FOUNDATION

Our approach is based upon recent extensions to detonation shock dynamics (DSD) theory, the current status of which are addressed elsewhere in these proceedings.[4] We give only a brief summary here to motivate the connection.

DSD is an approximation to the reactive Euler equations that allows numerically efficient tracking of curved detonation waves. Full numerical simulation involves calculating the reaction zone structure, for which one must specify both the "mixture" equation-of-state (EOS) and the reaction rate for the burning explosive. This is doubly problematic because a) the mixture EOS and the reaction rate are poorly known, and b) calculating the reaction zone is very computationally intensive.

DSD avoids both problems through the use of an *intrinsic relation*, which is a theoretically motivated mathematical expression relating the local wave shape to its local motion. The intrinsic relation coefficients for a given HE depend upon both its EOS and reaction rate; however, no *explicit* knowledge of the two is necessary. Rather, the intrinsic relation is calibrated directly from suitable detonation experiments.[6]

A convex detonation shock is causally insulated from the downstream world by a sonic surface. This attribute makes an intrinsic relation (which knows only about conditions at the shock front, and nothing of downstream world) mathematically well-posed. An initiating shock lacks this condition over much of its run-up, and is generally driven by both reactive heat release and back boundary motion. The extreme case is that of an inert shock, which is driven entirely by back boundary motion. Here Whitham's shock dynamic theory[7] (the predecessor to DSD) is nevertheless a useful approximation in many cases.

DSD is actually a hierarchy of models ordered by the complexity of the intrinsic relation. The zeroth approximation is Huygens' construction. In the first approximation κ, the total local shock curvature, depends upon D_n, the corresponding normal velocity component. Any model using a higher-order intrinsic relation (involving temporal and spatial derivatives of κ and D_n) has been called an *extended* model.

In the simplest extended models, the intrinsic relation for $\kappa = 0$ (a plane wave) relates D_n to the shock acceleration $\mathrm{d}D_n/\mathrm{d}t$—which amounts to a simple model for shock initiation. The assumption that this *acceleration function* is the same for all shock inputs is equivalent to the SCI model. Thus one could say that extended DSD has a Forest Fire-like initiation model.

In their extensive paper on extended DSD theory, Yao and Stewart[8] compute a theoretical intrinsic relation assuming an ideal gas EOS, and Arrhenius kinetics with high activation energy. When applied to a plane wave ($\kappa = 0$), a simplified version of the Yao-Stewart equation (in which higher order terms are neglected) provides a good launching point for applying the extended DSD to shock initiation.

THE ACCELERATION FUNCTION

In the (κ, D_n, dD_n/dt) level of the extended theory, with □ set to zero, the Yao-Stewart (Y-S) intrinsic relation reduces to the expression

$$\frac{a}{a_m} = \left(\frac{D-U}{D-U_m}\right)\exp\left[\frac{U-U_m}{D-U_m}\right]. \qquad (1)$$

We adopt a slightly different notation than is used in the DSD literature, one that is descriptive of this particular problem. We denote the shock velocity by U, the shock acceleration by a, and the steady Chapman-Jouguet (c-j) velocity by D. Generally D is a fitting parameter, but it may be specified as a constraint if it is sufficiently well known from rate stick experiments. The other two fitting parameters are likewise chosen to have physical significance: a_m is the peak acceleration; U_m is the velocity at which it occurs.

Figure 1 plots eqn. 1 in dimensionless coordinates, for three values of the shape parameter U_m/D. A shock inserted at speed U_0 traces the middle curve to D as indicated by the arrows. The acceleration is finite for $U < D$. This reflects the assumed Arrhenius reaction rate, which, though it may be very small, is never identically zero. The acceleration is small at velocities near the bulk sound speed C, but not necessarily (depending upon U_m/D) vanishingly so. This has important implications to be discussed later.

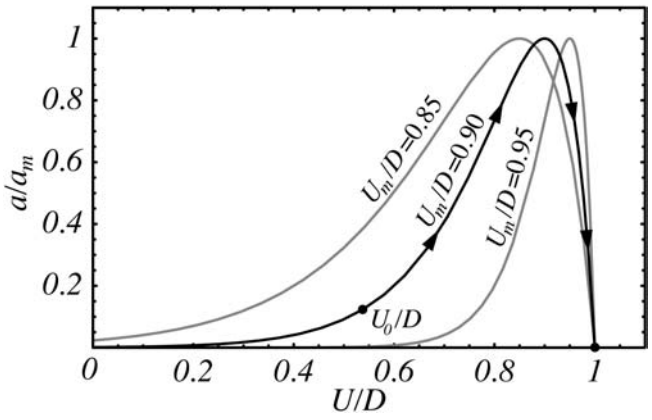

FIGURE 1: PLOT OF THE Y-S ACCELERATION FUNCTION, FOR THREE VALUES OF U_m/D. THE SHOCK TRAJECTORY FOLLOWS THE ARROWS IN TIME.

INTEGRAL SOLUTIONS TO $a[U]$

We now illustrate how best to obtain a fitting function $x[t]$ from a generating function $a[U]$, using eqn. 1 as an example. The elapsed time and distance of the shock, for a shock input velocity U_0, are given by the integrals

$$t\,[U;\,U_0\,] = \int_{U_0}^{U} \frac{\mathrm{d}\xi}{a[\,\xi]};\; x\,[U;\,U_0\,] = \int_{U_0}^{U} \frac{\xi\,\mathrm{d}\xi}{a[\,\xi]}. \qquad (2)$$

Equations 2 comprise a parametric solution for the shock trajectory in terms of U. This type of solution is fine for plotting, but is not accommodated by standard data fitting packages. For the Y-S equation, eqn. 2a integrates to:

$$t[U;\,U_0\,] = \left(\frac{D-U_m}{a_m\,\mathrm{e}}\right)\times \left(\mathrm{Ei}\left[\frac{D-U_0}{D-U_m}\right] - \mathrm{Ei}\left[\frac{D-U}{D-U_m}\right]\right), \qquad (3)$$

and eqn. 2b integrates to:

$$x^*[U_0] = \left(\frac{(D-U_m)^2}{a_m}\right)\times \left(\exp\left[\frac{U_m-U_0}{D-U_m}\right] - \exp\left[\frac{U_m-Ud}{D-U_m}\right]\right) + \left(\frac{D(D-U_m)}{a_m\,\mathrm{e}}\right)\left(\mathrm{Ei}\left[\frac{D-U_0}{D-U_m}\right] - \mathrm{Ei}\left[\frac{D-U_d}{D-U_m}\right]\right). \qquad (4)$$

Ei[z] is the *exponential integral function*,

$$\mathrm{Ei}[z] = \int_{-z}^{\infty} \frac{\exp[-\xi]}{\xi}\,\mathrm{d}\xi. \qquad (5)$$

Next we eliminate U to obtain a function $f[x,\,t]$ =0. For the Y-S equation, we find that

$$1 + \ln\left[\exp\left[\frac{U_m-U_0}{D-U_m}\right] - \frac{a_m(x-D\,t)}{(D-U_m)^2}\right] = \mathrm{Ei}^{-1}\left[\mathrm{Ei}\left[\frac{D\,\text{-}U_0}{D\,\text{-}U_m}\right] - \frac{\mathrm{e}\,a_m\,t}{D-U_m}\right]. \qquad (6)$$

The final step is to solve for $t[x]$ or $x[t]$, either of which can be used to directly fit data. For Y-S,

$$x[t;\, U_0] = D\,t - \left(\frac{(D-U_m)^2}{a_m}\right)\times \qquad (7)$$

$$\left(\exp\left[\frac{D-U_0}{D-U_m}\right] - \exp\left[\mathrm{Ei}^{-1}\left[\mathrm{Ei}\left[\frac{D-U_0}{D-U_m}\right] - \frac{a_m\,t}{D-U_m}\right]\right]\right)$$

One finds that these three steps can be performed only for certain simple expressions for $a[U]$. In some cases only the first step is possible, and in others two out of three. When a full analytic solution is possible, it is often in terms of special functions and their inverses, as is the case for eqn. 1. This poses no problem, so long as all functions are known to the computing environment. Otherwise, they must be defined.

For equations allowing a subset of the above solution steps, or if undefined special functions are generated, then it is generally easiest to numerically compute the desired solution directly from $a[U]$. For example, to compute $x[t]$ one would solve the following second order ODE:

$$\ddot{x}[t] = a[\dot{x}[t]];\;\; x[0]=0;\;\; \dot{x}[0]=U_0, \qquad (8)$$

which modern mathematics packages will solve almost instantly by a single command. With modest effort, one may manually input trial parameters and iterate to achieve a good fit. Otherwise, a least squares analysis will generally require some programming. In our case we constructed a simple *Mathematica*® fitting algorithm based on eqn. 8.

SINGLE CURVE INITIATION MODEL

The single curve initiation model (SCI) assumes that all shock trajectories follow the same "master build-up" curve. The idea is most frequently expressed in the *x-t* plane, where all trajectories centered on (t^*, x^*) are identical regardless of U_0. The *x-t* master curve can be transformed to other planes, for example $a[U]$, $U[t]$, and $U[x]$. In fact we shall find these planes (and particularly $a[U]$) more useful in appraising the SCI model than *x-t*, which turns out to be too insensitive a measure.

If formal SCI assumption is simple, the physical implications are less obvious. The simple thought experiment illustrated in Fig. 4 is illuminating. In Fig. 4a, an explosive sample is impacted by a flyer-plate of velocity u_1, which generates a shock of velocity U_1. After a time δt the shock has accelerated, due to reaction in the shocked material, to a greater speed U_2 (Fig. 4b). In Fig. 4c an identical sample is shocked by a flyer of speed u_2, to an *initial* speed U_2. SCI assumes that cases 4b) and 4c) behave *identically* as the shock accelerates from U_2 to D, for *all* possible combinations of u_1 and δt. This can only happen if the shock in 4b) is unaffected by the additional layer of reacting material. This in turn implies that reaction is concentrated near the shock front (as for the steady detonation), or that a sonic surface promptly develops that insulates the shock from the downstream reacting material. Consequently short and sustained shocks behave the same in the SCI model.

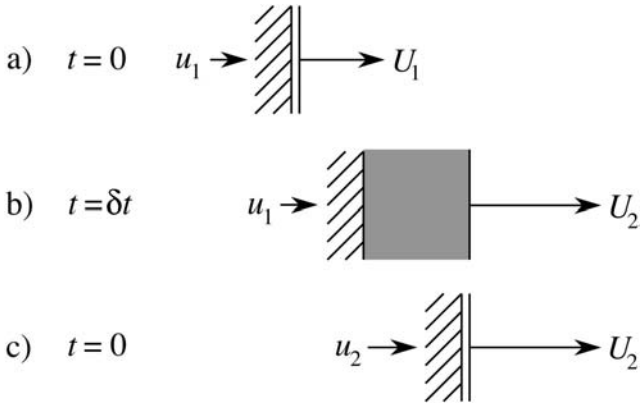

FIGURE 2: THOUGHT EXPERIMENT TO ILLUSTRATE SCI MODEL PROPERTIES.

The SCI picture does not mesh well with our physical understanding of the initiation process. In fact, the initiation of a physically homogeneous explosive is thought to be much the opposite situation. In that case the shocked explosive self-heats, or "cooks", for an induction time Δt before reaction runs away. Thermal explosion then begins near the back boundary where material has cooked the longest. An induction locus then advances according to a lighting-time schedule set by the input shock. The prescription is that the induction locus

follows the shock at the same speed U_0, a distance $U_0 \Delta t$ behind. Soon heat release couples with the mechanics, transforming the thermal disturbance into a pressure wave that overtakes the shock. For sufficiently large $U_0 \Delta t$ the secondary wave will itself steepen into a shock, and will upon overtake impulsively accelerate the lead wave past the c-j velocity, which the latter then approaches asymptotically from above. Generally initiation is said to be "homogeneous" if the shock velocity overshoots, and "heterogeneous" otherwise.

In contrast, heterogeneous explosives initiate only by the aid of energy localization and "hot spots". When a hot region is created in a shocked PBX, there is a brief moment of competition between heat generation and loss. If reaction wins it does so quickly. This is a step toward the ideal SCI behavior outlined in Fig. 4. On the other hand, reaction does not necessary *finish* quickly, as hot spot initiated-reaction must fill in to consume the surrounding material.

Measured PBX initiation behavior is basically consistent with this generic reasoning about hot spots. PBX's do not exhibit overshoot, which implies that any overtaking disturbance is diffuse. This conclusion is supported by magnetic particle velocity gauges, which show that a broad "hump" of reacting flow develops that grows, sharpens, and moves forward to catch the shock. Ultimately it evolves into the steady reaction zone structure.

THE KINEMATIC SCI POP PLOT

One nice feature of the SCI model is that the $U[t]$ and $U[x]$ master curves can be transformed to *kinematic* Pop plots, a term we've coined for $t^*[U_0]$ or $x^*[U_0]$. (One can easily transform to the traditional *dynamic* Pop plot, $t^*[P_0]$ or $x^*[P_0]$, if the inert Hugoniot is known.) In principle, one can estimate the kinematic Pop plot from a single initiation record or, conversely, calculate shock trajectories from the Pop-plot.

The transformation from the laboratory to the Pop plot frame is illustrated in Fig. 5. For every value of the input shock velocity U_0 there is a transition point x^*, defined by some initiation criterion $U = U_d$, which also lies on the master curve. The locus of all possible (U_0, x^*) pairs therefore map out the master curve. We need only change our coordinate system to adopt the Pop plot interpretation. The new coordinate system is shown in Fig. 5a, and the completed transformation is shown in Fig. 5b. If $t[U] = f[U]$, then the transformation rule is $t^*[U_0] = f[U_d] - f[U_0]$. Likewise if If $x[U] = g[U]$, then the transformation rule is $x^*[U_0] = g[U_d] - g[U_0]$. For the Y-S equation the kinematic Pop plot $t^*[U_0]$ is given by:

$$t^*[U_0] = \left(\frac{D - U_m}{\mathrm{e}\, a_m}\right) \times \left(\mathrm{Ei}\left[\frac{D - U_0}{D - U_m}\right] - \mathrm{Ei}\left[\frac{D - U_d}{D - U_m}\right]\right). \qquad (9)$$

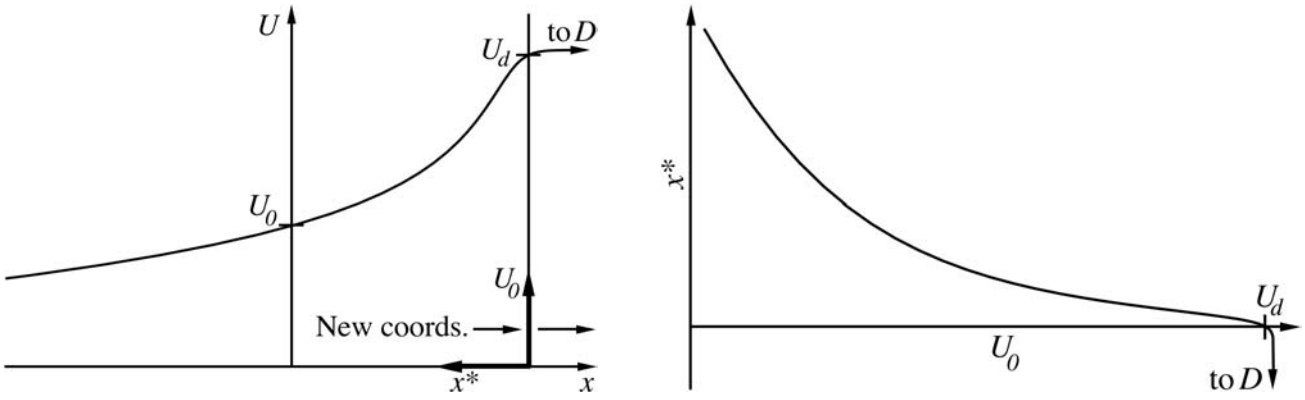

A) SCI VELOCITY MASTER CURVE **B) KINEMATIC SCI POP PLOT**

FIGURE 3. TRANSFORMATION FROM THE VELOCITY MASTER CURVE TO THE KINEMATIC SCI POP PLOT. THE COORDINATES ARE LINEAR.

Likewise, the result for $x^*[U_0]$ is

$$x^*[U_0] = \left(\frac{(D-U_m)^2}{a_m}\right)\times \left(\exp\left[\frac{U_m-U_0}{D-U_m}\right]-\exp\left[\frac{U_m-U_d}{D-U_m}\right]\right)+ \left(\frac{D(D-U_m)}{a_m\,\mathrm{e}}\right)\left(\mathrm{Ei}\left[\frac{D-U_0}{D-U_m}\right]-\mathrm{Ei}\left[\frac{D-U_d}{D-U_m}\right]\right). \quad (10)$$

The definition of the threshold U_d is a matter of preference. $U_d = U_m$ and $U_d = \eta D$ are both obvious choices. The first definition is aesthetic because it has no arbitrary parameters; the second is attractive because for fixed D, the upper Pop plot termination does not depend upon the fitting parameters.

FITS TO PBX 9501 AND PBX 9502 DATA

We now fit eqn. 1 to recent PBX 9501 and PBX 9502 gas gun data. Existing shots for each explosive were designed to generate three nominal input pressures that resulted in short, medium, and long runs in the fixed sample length. We have selected the nicest data set in each of the six categories for detailed study.

In fitting each HE, we begin by assuming that SCI holds. That is, we jointly fit the three records to a common $a[U]$ by keeping the parameters U_m and a_m the same for all sets. U_0 is of course different for each sample. D was constrained to 8.80 mm/μs for PBX 9501 and 7.65 mm/μs for PBX 9502. (The true c-j velocity for PBX 9502 is poorly known due to an upturn in the diameter effect curve as $1/R$ -> 0. Values as high as 7.8 mm/μs have been extrapolated; the present value is that which best fits the current data.) We also allowed a separate offset X_0 for each record, as the magnetic gauges had a placement tolerance of roughly 100 μm within the sample. Best-fit values greater than about 100 μm were considered suspicious, but typically the calculated offsets were of this order or less.

To test for departure from SCI, we performed a second series of fits in which U_m and a_m were allowed separate values for each record. The best-fit parameters from the first (SCI) fit were used as starting values for the individual fits. This two-step procedure helped to ensure that the different records didn't get trapped in different local minima of the merit function.

The three PBX 9501 data sets are plotted in Fig. 2. The *x-t* points were generated by magnetic *shock tracker* gauges, which are described elsewhere in these proceedings.[3] The individual fits to the data are superimposed, and the fit quality is excellent in all three cases. The standard deviation of the fit residuals σ (magnified 10x in the plots) were 17, 27, and 16 μm respectively. The three PBX 9502 data sets are plotted in Fig. 3. There were multiple gauge packages in these shots, and a small interleaving error is apparent in the fit residual pattern. This increased the σ's (which were 37, 43, and 45 μm respectively) relative to the PBX 9501.

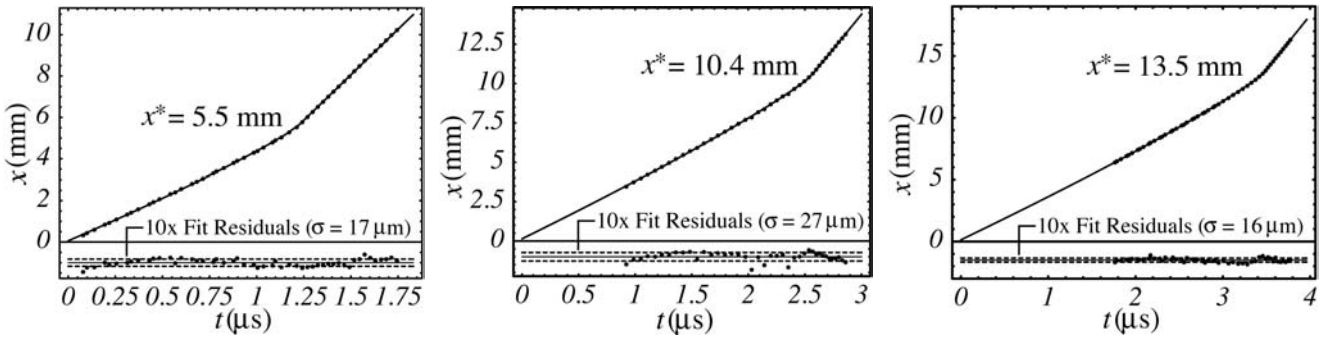

A) SHORT RUN (#1154) B) MEDIUM RUN (#1179) C) LONG RUN (#1165)

FIGURE 4: INDIVIDUAL FITS TO THREE PBX 9501 SHOCK INITIATION DATA SETS.

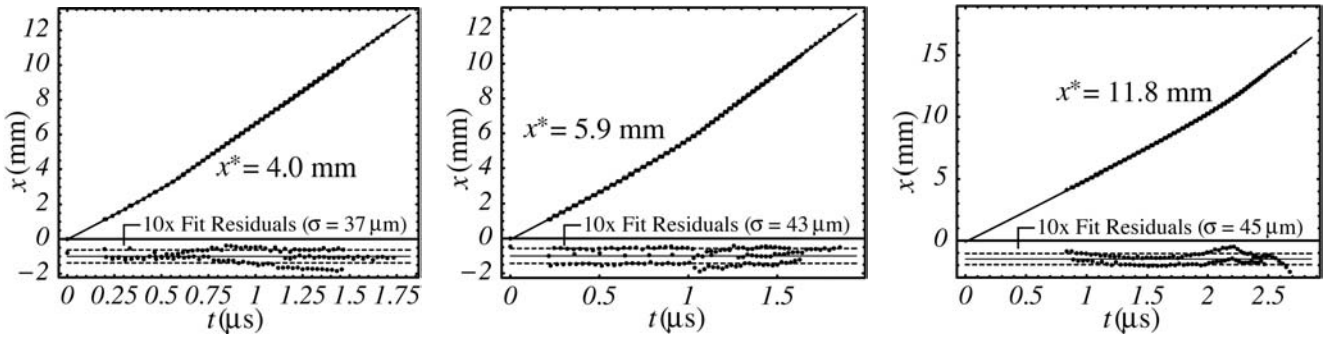

A) SHORT RUN (#2s-85) **B) MEDIUM RUN (#2s-86)** **C) LONG RUN (#2s-70)**

FIGURE 5: INDIVIDUAL FITS TO THREE PBX 9502 SHOCK INITIATION DATA SETS.

Figure 6 plots $a[U]$ corresponding to the fits of Figs. 4 and 5. For both HE's the functions are ordered according to U_0 or, alternatively, x^*. This is compelling evidence that build-up does not strictly follow the SCI model. Moreover, the departure is sensible based on the previous discussion: weaker inputs and longer runs allow the reacting flow more time and distance to organize and steepen into an overtaking wave.

There are perhaps two reasons why we detect SCI breakdown where most previous studies have not. The first is improved data quality; the second is that $a[U]$ is a sensitive plane. In fact, the differences it exposes may be *too* sensitive to affect many engineering calculations. To test this aspect we compared the quality of x-t fits for individual records (i.e., Figs. 4 and 5), to those obtained under SCI-constraint. The medium-run fits were virtually unchanged, since the SCI fits reflect the average behavior of the sets. The short and long-run fits were still very good. The SCI σ's were 26, 27, and 20 μm for PBX 9501 (a 22% average increase) and 38, 43, and 47 μm for PBX 9502 (a 2.4% average increase). The smaller increase for 9502 is likely due to the uncertainty introduced by gauge interleaving.

We have noted that eqn. 1 has finite acceleration for all $U < D$. This means that an acoustic wave eventually runs to detonation—even for PBX 9502! In reality, a PBX subjected to a weak shock relies on the hot spot mechanism to initiate reaction. That process is completely absent for acoustic waves, and for elastic waves as well. Hot spots form only when the shocked stress level exceeds the material strength, such that the initially heterogeneous compact homogenizes in a manner that produces localized energy dissipation. Evidently, initiation cannot occur below U_h, the shock velocity at the *Hugoniot elastic limit*. The distinction has little effect on the present model, as Fig. 6 shows that U_h and C are nearly equivalent[9,10].

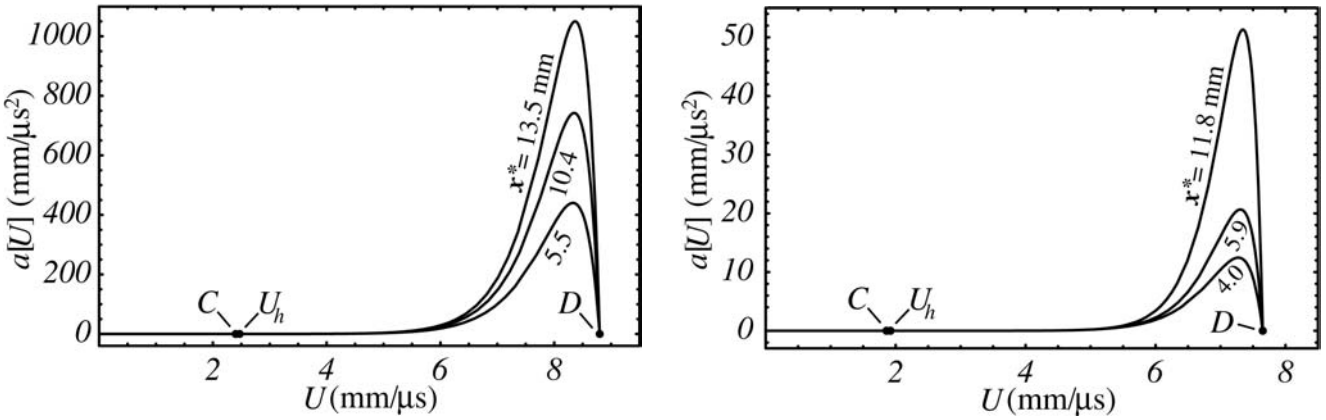

A) PBX 9501 **B) PBX 9502**

FIGURE 6: ACCELERATION FUNCTIONS FOR THE X-T FITS OF FIGS. 4 AND 5.

On Inert Hugoniot Accuracy

The inert Hugoniot curve is constructed from a collection of (u_0, U_0) data pairs. U_0 is the initial shock velocity, a fitting parameter in this analysis. u_0 is the input particle velocity, which for a traditional wedge test is inferred by an impedance-matching calculation. One gets a single Hugoniot point per traditional wedge test.

Whether the data comes from a firing site or a gas gun, the traditional method for inferring U_0 is to fit a straight line to the early shock trajectory. Since the goal is to construct an *inert* Hugoniot, one wishes to obtain the measurement over a short time and distance, before reaction accelerates the shock and spoils the result. The dilemma is that measurements over short times and distances lead to large uncertainties in the slope.

Fitting a straight line to an accelerating curve leads to an overestimate of the initial slope U_0. From the shape of $a[U]$ it is clear that the effect becomes progressively worse as U_0 increases. The present method computes the local value of U_0 from a fit that follows the general trend. As expected, this method gives consistently smaller, and presumably more accurate, values for U_0 than does the traditional straight-line method.

Comparison of the Real and SCI Pop Plots

Our best estimate of the Pop plot comes from applying eqns. 9 and 10 to the individual fits. This gives a single point for each record. The SCI Pop plot curve is given by eqns. 9 and 10 with the SCI fitting parameters. If SCI holds then the two should overlay.

Figure 7 shows the comparison, for U_d = 0.99 D. The dotted curves are the SCI Pop plots. These give a predicted run distance $x^*[U_h]$ of 7.6 cm for PBX 9501, and 18 m for PBX 9502. The latter is probably acceptably large, but the former incorrectly predicts a safety problem. In reality we've argued that $a[U_h]$ should be identically zero. One can certainly devise analytic forms that satisfy this constraint. Given the success of the Y-S equation, the most sensible fix is to add a term equation as follows:

$$\frac{a}{a_m} = \left(\frac{D-U}{D-U_m}\right) \times \left(\exp\left[\frac{U-U_m}{D-U_m}\right] - \exp\left[\frac{U_c-U_m}{D-U_m}\right]\right), \qquad (11)$$

where $U_c > U_h$ is a cutoff velocity. The correction provided by the additional term is shown by the solid lines in Fig. 7. Most of the curve is essentially unchanged, but now the Pop plot asymptotes to infinite run as U_c is approached. The dashed curve is the best fit to the real Pop plot points. The SCI and "real" curves deviate in qualitatively the same way for both HE's, the SCI Pop plot being steeper than the real one.

This small modification of eqn. 1 precludes any analytic solutions, and one must proceed numerically as outlined earlier. One consolation is that the fitting parameters are almost unchanged. One can perform fits on eqn. 1, and apply the parameters to eqn. 11. with reasonable accuracy. For precise results the fit should be reevaluated.

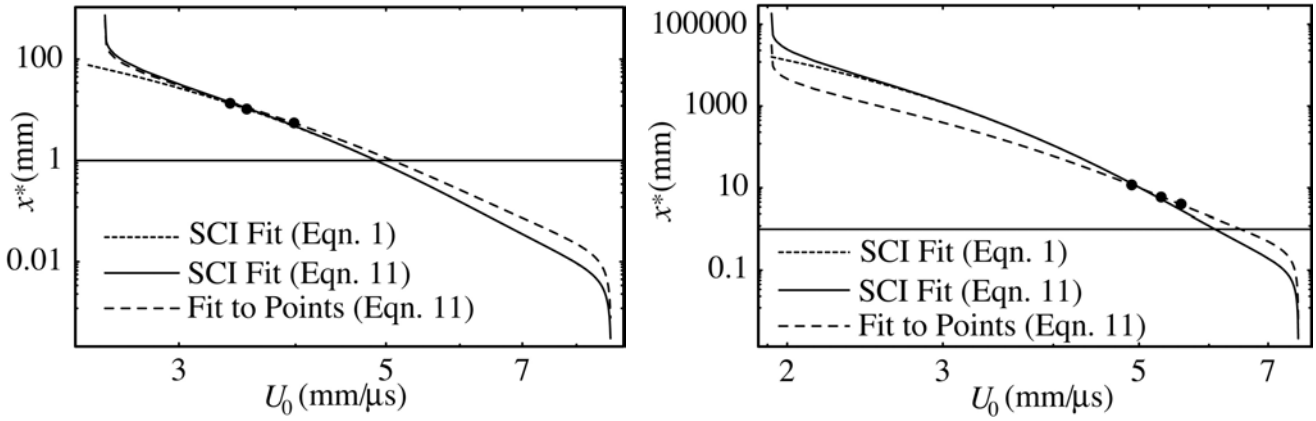

A) PBX 9501 **B) PBX 9502**

FIGURE 7: COMPARISON OF REAL AND SCI POP PLOTS FOR PBX'S 9501 AND 9502.

SCALING CONSIDERATIONS

In Fig. 8 we overlay the SCI acceleration curves for PBX's 9501/2, normalized by their full-scale values D and a_m. This allows us to examine shape differences, parameterized (as in Fig. 1) by U_m/D. The two curves very nearly overlay, suggesting that by proper scaling one can deduce a nearly universal heterogeneous initiation law.

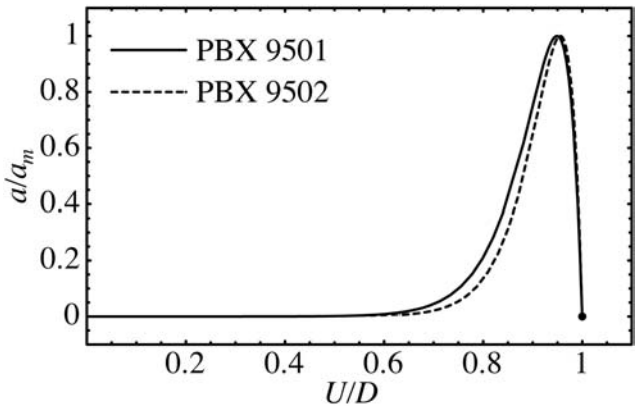

FIGURE 8. SCALED SCI Y-S ACCELERATION CURVES FOR PBX'S 9501 AND 9502.

The difference between PBX's 9501/2 is in many ways modest. 9502 has 30% less energy, detonates 13% slower, and is about 20% deficient in detonation pressure. The big difference between the two is sensitivity, which is closely related to the c-j reaction zone thickness δ. Though it is poorly known, failure diameter tests indicate that $\delta_{9502} = O(10)\ \delta_{9501}$. Likewise, the only large difference between the two $a[U]$ functions is that $a_{m9501} \sim 10\ a_{m9502}$. Evidently a_m and δ are related.

From a dimensional analysis viewpoint the fundamental length, velocity, and acceleration scales are δ, D, and a_m respectively. We therefore conclude that $a_m \sim D^2/\delta$—which reconciles the above two factors of 10. The proportionality constant will be of order unity if we have chosen the right "yardstick" by which to measure a_m. Assuming this to be true, we find that $\delta_{9501} = O(100)$ μm and $\delta_{9502} = O(1)$ mm, in agreement with other estimates for these HE's.

We have shown that SCI is a reasonable approximation for PBX's 9501/2 individually. Figure 8 further suggests that *both* HE's can be jointly fit using SCI and the above scaling arguments. Let $a_m = D^2/\Delta$, where Δ as an effective reaction zone thickness that we've argued is of order the true c-j value δ. D is specified for each explosive as before, and Δ is a separate fitting parameter for each HE. The shape factor U_m/D is a fitting parameter common to both explosives. U_0 and X_0 are different for the 6 shots, making 15 free parameters total. The exercise is performed for eqn. 1; to use eqn. 11 one would fix $U_c \sim U_h$, and use $(U_m - U_c)/(D - U_c)$ as the common shape factor rather than U_m/D.

The result is that $\Delta_{9501} = 75$ μm, $\Delta_{9502} = 2.7$ mm, and $U_m/D = 0.95$. The mean σ for the PBX 9501 shots is 41 μm—a 71% increase over the SCI fit to 9501 alone, but still very good. The corresponding error for the PBX 9502 shots is 42 μm, unchanged from the SCI fit to 9502 alone (which again is likely related to gauge interleaving). The velocity overshoot exhibited by purely homogeneous initiation is a departure from the "universal" law. Modest overshoots can be fit by eqns. 1 or 11 with minimal error.

THE HETEROGENEITY PARAMETER

The success of the joint fitting exercise indicates that what is called "homogeneous" vs. "heterogeneous" initiation behavior is really only a matter of scale. That is, it depends on how large x^* is compared to δ. In a wedge test the sample length, and hence the upper bound on x^*, is fixed at a practically achievable value (a few centimeters). Consequently x^*/δ is an order of magnitude greater for PBX 9501 than for 9502, and we observe different initiation regimes.

To quantify the effect we define the dimensionless *heterogeneity parameter Ht*, which measures U_0 relative to the endpoints of $a[U]$:

$$Ht \equiv \frac{U_0 - U_h}{D - U_h}. \qquad (11)$$

Ht is zero for perfectly homogeneous behavior, and unity for perfectly heterogeneous behavior. It is independent of the form chosen for $a[U]$ (a practical advantage), but implicitly assumes the type of similarity discussed above.

Figure 9 shows how the six cases order with respect to explosive type and run distance. PBX 9501 is rather homogeneous, and PBX 9502 is slightly heterogeneous. Shorter runs are more heterogeneous than longer ones.

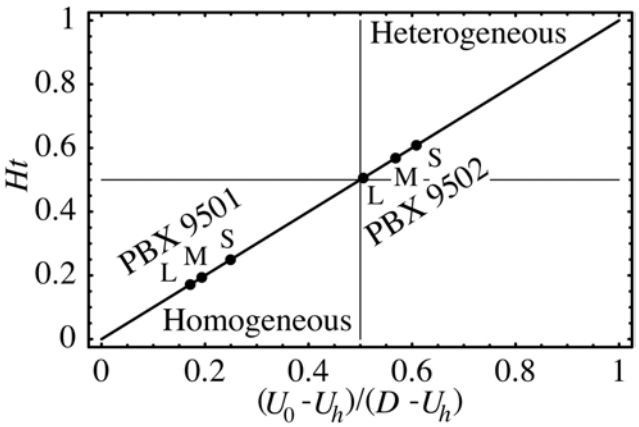

FIGURE 9. HETEROGENEITY PARAMETER FOR PBX 9501 AND PBX 9502.

OTHER ACCELERATION FUNCTIONS

We have explored several empirical forms for $a[U]$ to determine if the Y-S equation has "magical" properties. The result is that most any function of the right general shape will nicely fit individual *x-t* records; however, similar functions differ in their ability to jointly fit multiple records, especially when U_c is pinned to a physically realistic value. The modified Y-S form (eqn. 11) is as good as any we've found so far.

One also finds that the a_m value needed to get to the right distance at the right time depends strongly on the function shape. The Y-S equation predicts larger a_m values (by up to an order of magnitude) than most other forms we've tested. That it returns the expected value of δ from reasonable scaling arguments tempts one to favor Y-S over other forms, but that result was obtained by assuming the proportionality constant to be closer to unity than it need be.

The important lesson is that one should compare different explosives using the *same* form for $a[U]$. Then the relative values of a_m are meaningful, even if the absolute values are poorly known. Then if δ is measured for a reference explosive, then the a_m ratios can predict it for other explosives.

ACKNOWLEDGEMENTS

We are grateful to T. Aslam, J. Bdzil, B. Davis, A. Kapila, R. Rabie, S. Sheffield, and S. Stewart for useful discussions on shock initiation. We thank P. Howe and D. Idar for funding this work. We thank B. Miller of Wolfram research for advice about fitting with *Mathematica*. This work was supported by the United States Department of Energy.

REFERENCES

1. Campbell, A.W.; Davis, W.C.; Ramsay, J.B.; and Travis, J.R. *Shock Initiation of Solid Explosives.* Phys. Fluids, V. 4, No. 4 (1961)
2. Campbell, A.W.; Davis, W.C, and Travis, J.R. *Shock Initiation of Liquid Explosives.* Phys. Fluids, V. 4, No. 4 (1961)
3. Gustavsen, R.L.; Sheffield, S.A.; Alcon, R.R.; and Hill, L.G. *Shock Initiation of New and Aged PBX 9501 Measured with Embedded Electromagnetic Particle Velocity Gauges.* These proceedings.
4. Bdzil, J.B.; Short, M.; Aslam, T.D.; Catanach, R.A.; & Hill, L.G. *DSD Front Models: Non-ideal Explosive Detonation.* These proc.
5. Mader C.L., & Forest, C.A.; *2D Homogeneous & Heterogeneous Detonation Wave Propagation.* LASL Rpt. No. LA-6259 (1976)
6. Hill, L.G.; Bdzil, J.B.; & Aslam, T.D.; *Front Curvature Rate Stick Measurements and Detonation Shock Dynamics Calibration for PBX 9502 Over a Wide Temperature Range.* 11th Symp (Int.) on Detonation (1998)
7. Whitham, G.B.; *Linear and Nonlinear Waves.* John Wiley & Sons (1974)
8. Yao, J., and Stewart, D.S.; *On the Dynamics of Multi-Dimensional Detonation.* JFM, V. 309 (1996) See eqn. 6.86.
9. Dick, J.J.; *Plane Impact Response of PBX 9501 and Its Components Below 2 GPa.* LANL Re-port No. LA-13426-MS (1998)
10. Dick, J.J.; Forest, C.A., Ramsay, J.B., and Seitz, W.L. *The Hugoniot & Shock Sensitivity of a Plastic-Bonded TATB Explosive PBX 9502.* J. Appl. Phys., V. 63, No. 10 (1988)